ACS APPLIED ENERGY MATERIALS

www.acsaem.org Article

# Nonflammable Gel Polymer Electrolyte with Ion-Conductive Polyester Networks for Sodium Metal Cells with Excellent Cycling Stability and Enhanced Safety

Tae-Hyun Park,[#] Myung-Soo Park,[#] A-Hyeon Ban, Yun-Sung Lee, and Dong-Won Kim*

Cite This: *ACS Appl. Energy Mater.* 2021, 4, 10153−10162 Read Online

ACCESS | Metrics & More | Article Recommendations | Supporting Information

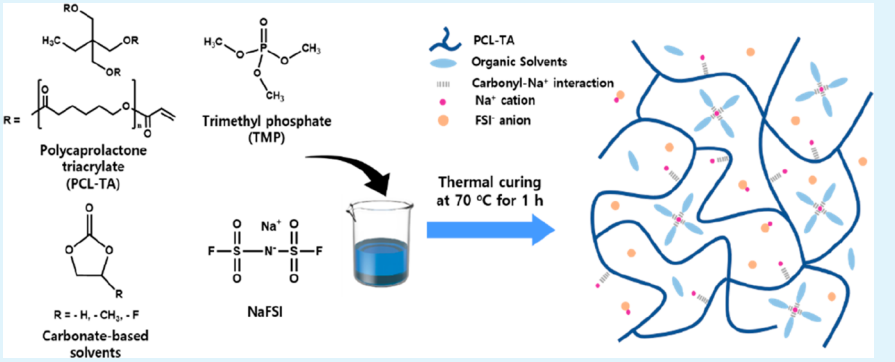


**ABSTRACT:** Sodium metal batteries have received a considerable amount of attention because of the low cost of Na resources and high theoretical capacity of Na metal. However, liquid electrolytes used in batteries cause safety problems such as fires and explosions under abnormal conditions. The uncontrolled dendritic Na growth in the cell also results in poor cycling stability. Herein, we report nonflammable gel polymer electrolytes (GPEs) synthesized by in situ cross-linking of a gel precursor containing ion-conductive polycaprolactone triacrylate. The GPE exhibits a high ionic conductivity of 6.3 mS $cm^{-1}$ because of the $Na^+$−carbonyl interactions and high segmental motion of polycaprolactone chains despite its three-dimensional network structure. The ion-conductive polymer networks effectively suppress the growth of Na dendrite by inducing uniform Na deposition on the Na electrode, resulting in improved interfacial characteristics of the Na electrode. The $Na/Na_3V_2(PO_4)_3$ cell employing GPE delivers high discharge capacities at high C rates and exhibits excellent cycling stability. Additionally, the superior thermal stability of GPE prevents a short circuit of the cell at high temperature, which allows safe operation of the $Na/Na_3V_2(PO_4)_3$ cells.

**KEYWORDS:** *sodium−metal battery, gel polymer electrolyte, ion-conductive polymer, polycaprolactone network, nonflammability*



## INTRODUCTION

As global warming is one of the most significant worldwide issues and many governments have proposed stringent regulations on fossil fuel use, the demand for sustainable energy sources and efficient energy storage technologies continues to grow. Lithium-ion batteries have become an indispensable part of our modern lives and have dominated the markets for mobile electronics and electric vehicles because of their excellent cyclability and high energy density.[1] Nevertheless, many researchers are exploring alternative energy storage systems because lithium resources are unevenly distributed and very limited, causing increasing battery costs for the near future.[2−4] In this respect, sodium-based batteries have garnered considerable interest due to the high abundance and low cost of sodium resources.[3−6] Moreover, material design strategies and characterization techniques for sodium batteries are similar to those of their lithium counterparts.[5,6]

Sodium-based batteries generally employ liquid electrolyte composed of organic solvents and sodium salt,[7−10] which raise safety issues such as fires and explosions under abnormal situations such as overcharging and short-circuiting.[11,12] In this regard, solid electrolytes are a promising candidate to solve the safety problems. Among them, solid-state polymer electrolytes have attracted a great deal of attention because of their design flexibility, absence of leakage, and good interfacial properties. Unfortunately, their low ionic conductivities at ambient temperature are a hurdle for their practical application.[13,14] In contrast, gel polymer electrolytes (GPEs) can be a more

**Received:** July 13, 2021
**Published:** September 10, 2021

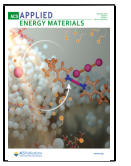




https://doi.org/10.1021/acsaem.1c02053
*ACS Appl. Energy Mater.* 2021, 4, 10153−10162

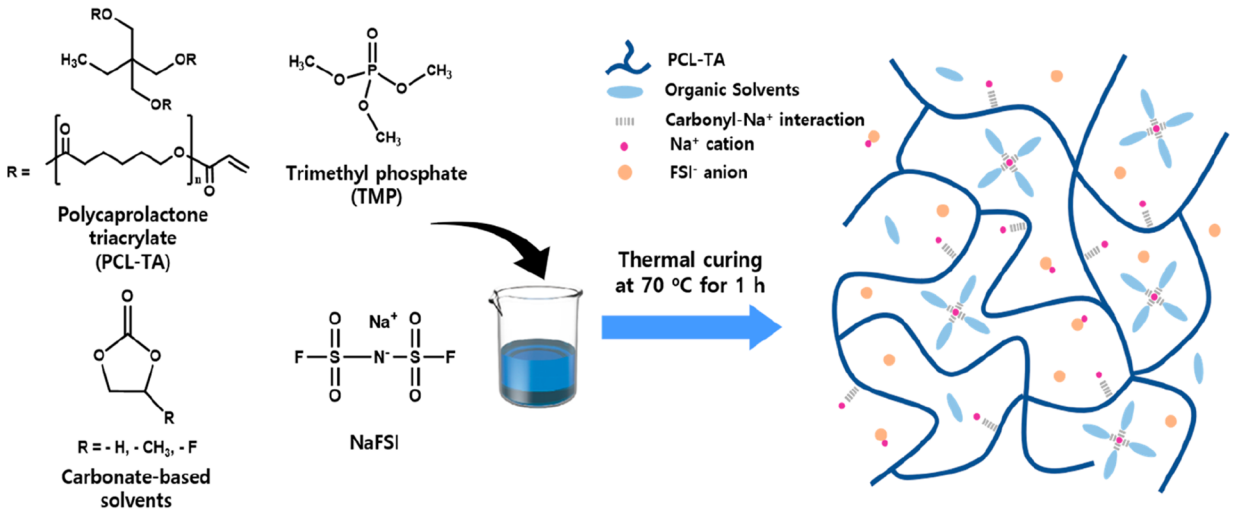


**Figure 1.** Schematic illustration of the synthesis of nonflammable GPE with ion-conductive polyester networks.

practical system for sodium batteries, considering high ionic conductivities, good interfacial characteristics toward electrodes, and effective encapsulation of organic solvents within the cell.[15−20] Another approach to address the safety issues is to use a nonflammable electrolyte.[21] As a flame-retardant additive, organic phosphorus compounds such as phosphates and phosphonates have been actively explored because of their excellent fire-extinguishing properties.[22−24] Although phosphate-based electrolytes exhibit nonflammability and high ionic conductivity, their electrochemical decomposition on the anode and formation of an unstable solid electrolyte interphase (SEI) have hindered their practical applications.[25] To solve these problems, many researchers have studied highly concentrated phosphate-based electrolytes, allowing the formation of a stable SEI layer on the anode by preferential decomposition of imide anions.[26,27] However, they cause critical concerns related to their high viscosity and costly alkali-metal salt.[28] Consequently, optimization of the phosphate content is necessary to minimize the detrimental decomposition of phosphate solvents.

In this study, a nonflammable GPE was synthesized by thermal curing of trimethyl phosphate (TMP)-containing liquid electrolyte using ion-conductive polycaprolactone triacrylate (PCL-TA) as a cross-linking agent. The GPE synthesized with 8 wt % PCL-TA and liquid electrolyte containing 15 vol % TMP exhibited nonflammability, non-fluidity, and a high ionic conductivity of 6.3 mS $cm^{-1}$ at room temperature. The high ionic conductivity arose from additional ion−polymer interactions and facile ion transport because of flexible polymer chains. Uniform $Na^+$ flux through the GPE and immobilization of organic solvents in the three-dimensional polymer networks effectively suppressed dendritic Na growth and solvent decomposition at the electrodes, resulting in improved cyclability of the Na electrode. As a result, the $Na/Na_3V_2(PO_4)_3$ cells employing the GPE exhibited high discharge capacity and excellent cycling stability. Additionally, the thermal safety of sodium metal cells was greatly enhanced by replacing liquid electrolyte with chemically cross-linked GPE.

## EXPERIMENTAL SECTION

**Materials.** TMP (≥99.0%), ethylene carbonate (EC, 99.0%, anhydrous), and propylene carbonate (PC, 99.7%, anhydrous) were purchased from Sigma-Aldrich. Fluoroethylene carbonate (FEC, battery grade) and *tert*-butyl peroxypivalate (t-BPP) were purchased from Enchem and Arkema, respectively. The organic solvents and t-BPP were dehydrated with 4 Å molecular sieve. Tetrahydrofuran (THF, >99.5%, anhydrous, TCI), acryloyl chloride (anhydrous, TCI), triethylamine (TEA, anhydrous, Sigma-Aldrich), and sodium bis-(fluorosulfonyl)imide (NaFSI, 99.7%, $H_2O$ < 20 ppm, Solvionic) were used as received. Polycaprolactone triol (PCL-triol, $M_n$ = 900, Sigma-Aldrich) was vacuum-dried at 60 °C for 12 h before use.

**Preparation of Gel Polymer Electrolyte.** PCL triacrylate (PCL-TA) was synthesized by nucleophilic acyl substitution reaction between PCL-triol and acryloyl chloride, as reported in our previous work.[29] A quaternary solvent mixture was composed of EC, FEC, PC, and TMP (40:20:40−*x*: *x*, by volume), and 0.8 M NaFSI was dissolved in the mixed solvent to prepare the liquid electrolyte. For the preparation of the GPE precursor, a proper amount of PCL-TA was added into the liquid electrolyte with t-BPP (1.0 wt % of PCL-TA) as a thermal initiator. Then the precursor was kept at 70 °C for 1 h to induce the thermal curing and obtain chemically cross-linked GPE, as schematically presented in Figure 1. Karl Fischer titration confirmed that the moisture content in the GPE was less than 25 ppm.

**Cell Assembly.** An active $Na_3V_2(PO_4)_3$ material was prepared by a sol−gel technique, as previously reported.[30] The $Na_3V_2(PO_4)_3$ cathode was composed of $Na_3V_2(PO_4)_3$, poly(vinylidene fluoride), and Ketjen black with a weight ratio of 80:10:10. The mass loading of active $Na_3V_2(PO_4)_3$ material in the cathode was about 10.0 mg $cm^{-2}$. The thickness and area of the sodium anode were 200 $\mu$m and 1.77 $cm^2$, respectively. A coin-type $Na/Na_3V_2(PO_4)_3$ cell was fabricated with the $Na_3V_2(PO_4)_3$ cathode, polyethylene (PE) separator (SK Innovation, 25 $\mu$m), and sodium metal anode. The GPE precursor was injected into the cell and in situ cross-linked at 70 °C for 1 h. All cells were assembled in the Ar-atmosphere glovebox.

**Characterization and Measurements.** $^1$H NMR spectra were obtained using a VNMRS 600 MHz spectrometer (Agilent Technologies). Acetone-$d_6$ was used as a solvent with tetramethylsilane as a reference. The viscosity of the liquid electrolyte was determined using a viscometer at room temperature. A flammability test of liquid electrolyte was performed by exposing a glass fiber separator soaked with liquid electrolyte to a torch flame. The stainless steel (SS) symmetric cell with GPE (SS/GPE/SS) was assembled to measure the ionic conductivity of GPE. AC impedance of the cell was measured using an impedance analyzer (ZIVE MP1, Wonatech) at different temperatures in the frequency range of 10−$10^6$ Hz. Linear sweep voltammetry was performed using a platinum working electrode with sodium metal as the reference and counter electrodes at 1 mV $s^{-1}$ and 25 °C. Attenuated total reflectance Fourier transform infrared (ATR-FTIR) spectroscopy was carried out using a Nicolet


https://doi.org/10.1021/acsaem.1c02053
ACS Appl. Energy Mater. 2021, 4, 10153−10162

iS50 spectrometer. Raman spectra were obtained using a LabRAM HR Evolution Raman spectrometer with a 785 nm laser source. Galvanostatic cycling of the Na symmetric cells was carried out in the voltage range of −1.0 to 1.0 V at 0.5 mA $cm^{-2}$ and 25 °C for 2 h. The morphology and chemical composition of the sodium electrode were investigated by field-emission scanning electron microscopy (FE-SEM, JEOL JSM 6710F) and X-ray photoelectron spectroscopy (XPS, VG Multilab ESCA system, 220i). A cycling test for the Na/$Na_3V_2(PO_4)_3$ cell was performed in a voltage range of 2.5−4.0 V using a battery tester at 25 °C. To investigate the thermal safety of the Na/$Na_3V_2(PO_4)_3$ cell, it was charged to 4.0 V and kept at 140 °C. Then the open-circuit voltage of the cell was monitored as a function of storage time.

## RESULTS AND DISCUSSION

Figure S1 (Supporting Information) presents a schematic for the synthesis of PCL-TA, which was used as an ion-conductive cross-linking agent in this study. Ether-based cross-linkers have been usually used for the synthesis of chemically cross-linked GPEs.[31,32] However, their oxidative stability is too low to operate cells under high-voltage conditions. Hence, we synthesized an ester-based cross-linking agent because ester groups (−COO−) have high anodic stability and can solvate Na salts to produce a lot of free ions.[18,33] To confirm the structure of PCL-TA, we obtained the $^1$H NMR spectra of PCL-triol and PCL-TA (Figure S2). The proton peaks corresponding to (i), (j), and (k) in Figure S2b can be assigned to the vinyl protons in the acrylate group of PCL-TA, indicating that the −OH groups in PCL-triol were successfully substituted with acrylate groups.

Figure 1 illustrates the synthesis of cross-linked GPE using PCL-TA in the presence of NaFSI, TMP, and carbonate-based solvents (EC, PC, and FEC). The thermodynamic equilibrium was reached when forming 4sol−$Na^+$ complexes in the carbonate solvents such as EC, PC, and dimethyl carbonate (DMC).[34] The GPE has a three-dimensional network structure; thus, the organic solvents were effectively encapsulated in the cross-linked polymer network. In this GPE, two types of ion−dipole interactions ($Na^+$−polymer/$Na^+$−organic solvent) occurred to dissociate the NaFSI salt into free ions. The details of interactions in the GPE will be discussed with the spectroscopic analyses later.

The TMP content was optimized by measuring the ionic conductivity and flammability of liquid electrolytes with different compositions. The liquid electrolyte was 0.8 M NaFSI dissolved in EC/FEC/PC/TMP (40:20:40−$x$:$x$). Figure 2a shows the ionic conductivities and viscosities of the liquid electrolytes as a function of the TMP content at 25 °C. As shown in the figure, the ionic conductivity of the electrolyte was increased with increasing TMP content because of the low viscosity of TMP compared to carbonate solvents. Figure 2b presents photographic images of the liquid electrolytes subjected to the flammability test. When the content of TMP was less than 10 vol %, the electrolyte solution immediately caught fire and kept burning for a long time. In contrast, the electrolytes with TMP content higher than 15 vol % showed no ignition during prolonged exposure (>5 s) because large amounts of $[P]^•$ radicals generated from TMP effectively captured $[H]^•$ radicals during ignition to terminate the combustion chain reactions.[25,35] Unfortunately, phosphate-based solvents are known to electrochemically decompose and form the unstable solid electrolyte interphase on the anode.[25] Thus, minimizing the content of TMP is necessary to reduce these side effects. On the basis of the above results, 15 vol %

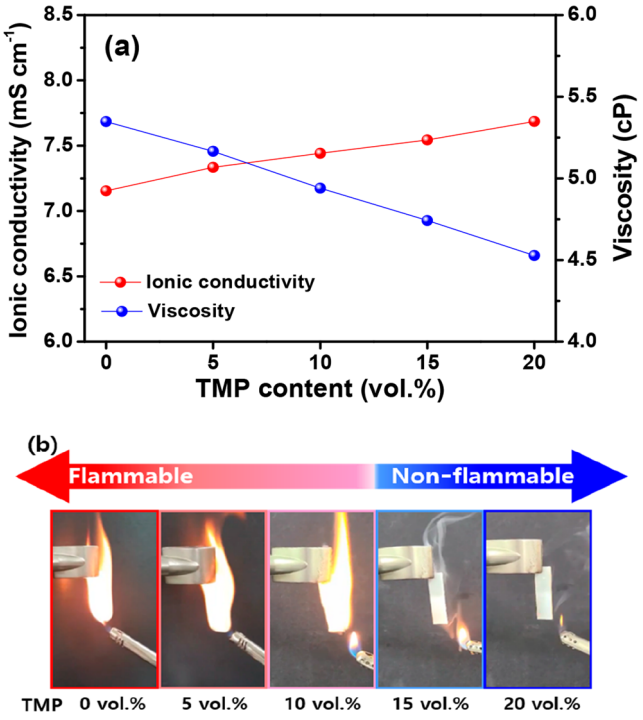


**Figure 2.** (a) Ionic conductivities and viscosities of the liquid electrolytes as a function of TMP content. (b) Photographic images of the liquid electrolytes subjected to the flammability test.

TMP was the minimum content to obtain a high ionic conductivity and nonflammability of the electrolyte. Thus, we chose the liquid electrolyte containing 15 vol % TMP for the preparation of GPEs in further experiments.

GPE was synthesized by a thermal curing of the gel precursor containing PCL-TA. Figure 3a presents a photographic image of the GPEs synthesized with different amounts of PCL-TA. Liquid flow was observed for the GPEs synthesized with PCL-TA contents less than 6 wt % because of the low cross-linking degree. On the other hand, the GPEs prepared with PCL-TA contents of 8 wt % or more became totally nonfluidic and showed no solvent exudation, demonstrating the formation of a three-dimensional polymer network that effectively encapsulates the organic solvents. Figure 3b presents the ionic conductivities of the GPEs as a function of PCL-TA content at 25 °C. As expected, the ionic conductivity gradually decreased with increasing PCL-TA content because the formation of three-dimensional networks with a high cross-linking degree reduced the ionic mobility in the GPE. Considering the results in Figure 3a,b, the optimum PCL-TA content for obtaining a robust polymer network and achieving high ionic conductivity was 8 wt %. Thus, we used the GPE synthesized with 8 wt % PCL-TA in additional experiments. The ionic conductivities of the electrolytes were measured in the temperature range of −15 to 75 °C. The activation energy ($E_a$) for ion conduction could be obtained from the Arrhenius plot in Figure 3c.[36] The activation energy of GPE (6.0 kJ $mol^{-1}$) is comparable to that of liquid electrolyte (5.8 kJ $mol^{-1}$) despite its three-dimensional network structure. The low $E_a$ of the GPE can be ascribed to the high concentration of free ions because of the additional $Na^+$−carbonyl interactions and fast ion transport facilitated by flexible polyester chains with a low glass transition temperature. The linear sweep voltammograms of the electrolytes are shown in Figure 3d.


https://doi.org/10.1021/acsaem.1c02053
ACS Appl. Energy Mater. 2021, 4, 10153−10162

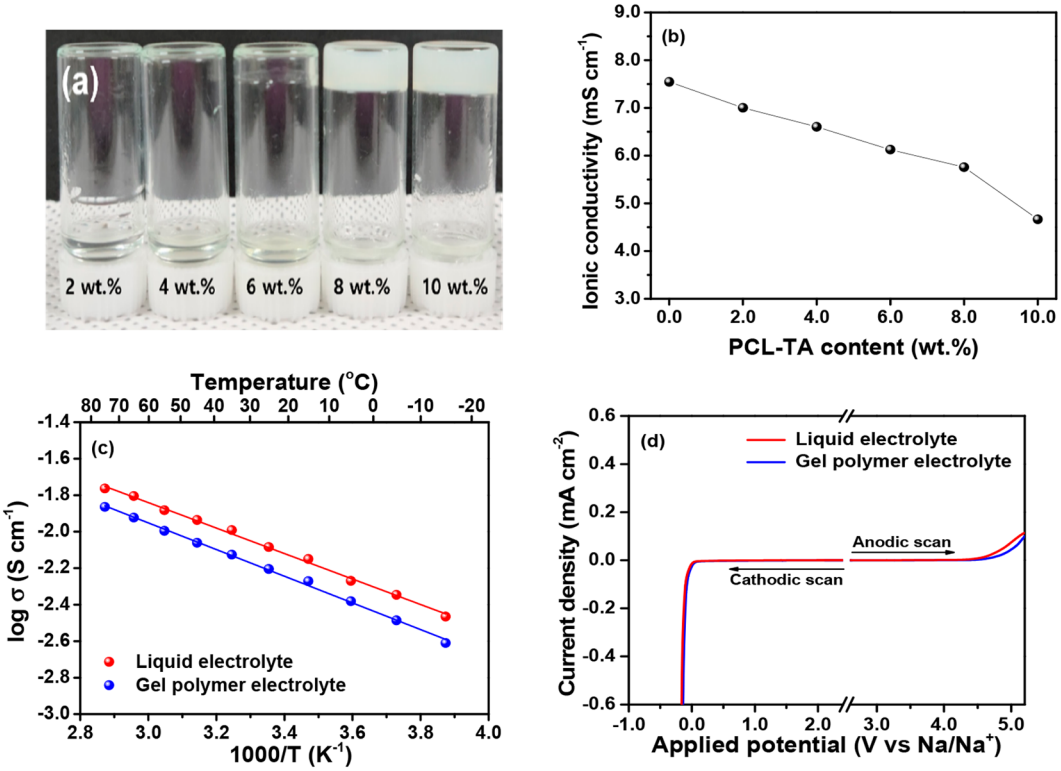


**Figure 3.** (a) Photographic image of GPEs cured with different amounts of PCL-TA. (b) Ionic conductivities of GPEs as a function of PCL-TA content. (c) Temperature dependence of ionic conductivities for liquid electrolyte and GPE. (d) Linear sweep voltammetry curves of liquid electrolyte and GPE at a scan rate of 1 mV $s^{-1}$ and 25 °C.

Both electrolytes showed no reductive decomposition prior to 0 V vs $Na/Na^+$ in the cathodic scan. The cathodic current observed below 0 V is attributed to the reductive deposition of sodium ions onto the Pt electrode. In the case of the anodic scan, neither electrolyte showed oxidative decomposition up to 4.5 V vs $Na/Na^+$. GPE exhibited a slightly higher anodic decomposition potential than the liquid electrolyte, indicating that the three-dimensional network structure suppressed the electrochemical decomposition of the liquid electrolyte because of the effective immobilization of organic solvents in the polymer networks. Photographic images of GPEs during the flammability test are presented in Figure S3. When GPE was exposed to a flame source for a long time, it did not burn, implying that GPE is fully nonflammable.

We investigated the ionic conductivity and flammability of GPEs as a function of TMP content, and the results are presented in Figure S4. The ionic conductivity of GPE was gradually increased with the TMP content. When the GPEs with a TMP content of 10 vol % or less were exposed to a flame source, they caught fire and kept burning. In contrast, the GPEs with the TMP content higher than 15 vol % showed no ignition because of the nonflammable nature of the liquid electrolyte, as previously discussed.

The ion−polymer interactions in the GPEs were examined by the FTIR and Raman spectroscopic analyses. The peaks at 1728 and 1712 $cm^{-1}$ in Figure 4a correspond to the free carbonyl (C═O) of the ester in PCL and the $Na^+$−carbonyl stretching of the ester groups in the PCL, respectively.[18] As the NaFSI concentration increased, the peak intensity at 1728 $cm^{-1}$ decreased and the peak intensity at 1712 $cm^{-1}$ gradually increased. The interaction between $Na^+$ ions and carbonyl groups in the polymer network induces additional dissociation of the NaFSI salt, which leads to the generation of large amounts of free $Na^+$ ions in the GPE. Additionally, the highly flexible polycaprolactone chains result in a high ionic mobility of free ions.[37] Parts (b) and (c) of Figure 4 present the Raman spectra of the liquid electrolytes and GPEs, respectively. The Raman peaks at 724, 734, and 742 $cm^{-1}$ can be assigned to free $FSI^-$ anions, contact ion pairs (CIP), and aggregates (AGG) of $FSI^-$ anions, respectively.[38] The other peaks in this region are also assigned in Table S1.[38−41] As shown in Figure 4d, the relative fraction of free $FSI^-$ anions in both electrolytes decreased with salt concentration. It is noticeable that GPEs showed higher relative fractions of free $FSI^-$ anions than did liquid electrolytes at all the salt concentrations. These results confirm that the PCL chains in the three-dimensional networks additionally solvate NaFSI salt and, thus, generate more free ions, which is advantageous for achieving facile electrochemical reactions at the electrode and electrolyte interface.

To compare the interfacial stability of the Na electrode in prolonged contact with electrolytes, we investigated AC impedance spectra of the symmetrical Na/electrolyte/Na cells as a function of storage time (Figure S5). The depressed semicircle observed in the medium- to low-frequency regions corresponds to the total interfacial resistance ($R_i$), which is a sum of the ionic resistance of the surface film on the Na electrode ($R_f$) and charge-transfer resistance ($R_{ct}$) at the electrode−electrolyte interface.[42] As clearly observed in Figure S4a, the Na/liquid electrolyte/Na cell exhibited a gradual increase of interfacial resistance with time, indicating the continuous formation of a resistive layer on the Na electrode due to side reactions between highly reactive Na metal and electrolyte solution. In contrast, the interfacial resistance in the cell with GPE eventually stabilized after initially increasing.


https://doi.org/10.1021/acsaem.1c02053
ACS Appl. Energy Mater. 2021, 4, 10153−10162

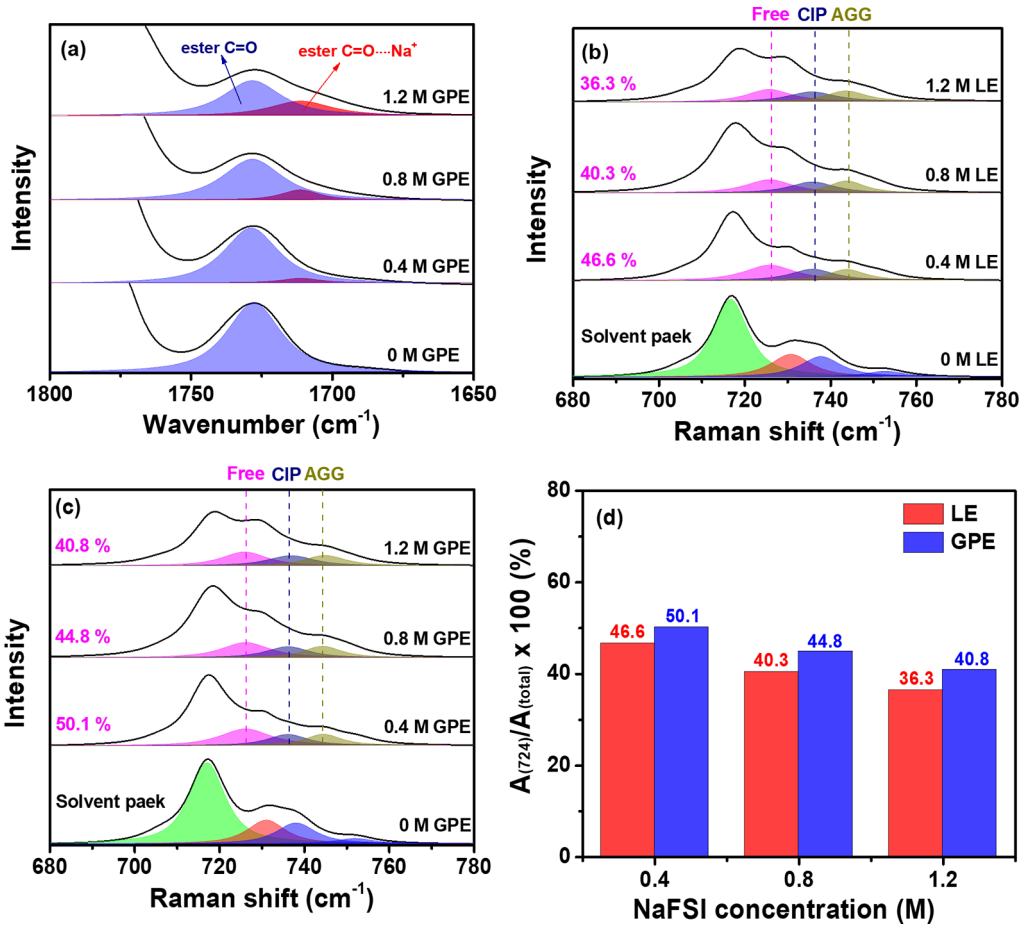


**Figure 4.** (a) ATR-FTIR spectra of GPEs with different NaFSI concentrations. Raman spectra of (b) liquid electrolytes and (c) GPEs. (d) Relative fractions of free $FSI^-$ anions in liquid electrolytes and GPEs as a function of NaFSI concentration.

These results imply that the three-dimensional network composed of PCL chains suppresses the electrolyte decomposition at the Na electrode by effectively trapping the organic solvents. The galvanostatic cycling of the symmetrical Na cells was performed at 0.5 mA $cm^{-2}$ to investigate the influence of the electrolyte on the Na plating/stripping behavior. Figure 5a shows the voltage profiles of the Na/electrolyte/Na cells employing different electrolytes during the plating/stripping of Na ($Na^+ + e \leftrightarrow Na$). In the cell with a liquid electrolyte, the voltage profile was considerably unstable, and the overpotential exceeded a preset voltage limit (−1.0 to 1.0 V) after 300 h. This unstable voltage profile is related to the irregular growth of Na dendrites and the vigorous SEI formation caused by continuous electrolyte decomposition at enlarged Na surfaces, as schematically illustrated in Figure 5b. The nonuniform SEI layer then induces inhomogeneous Na deposition and causes rapid growth of Na dendrites on the electrode during repeated cycling. This leads to the formation of a thick passivation layer composed of accumulated SEI residues and "dead Na," causing a large overpotential. In contrast, the Na/electrolyte/Na cell with GPE exhibited a lower overpotential and stable cyclability, indicating that GPE improved the plating/stripping behavior of the Na electrodes. As presented in Figure 5b, the suppressed electrolyte decomposition at the Na electrode induces the formation of a thin SEI layer and uniform Na deposition. The large amounts of free $Na^+$ ions in the GPE can also extend the Sand's time ($\tau$) when the $Na^+$ ion concentration decreases to zero at the electrolyte/electrode interface, which suppresses Na dendritic growth.[43,44] From these results, it can be said that the use of GPE can enhance the reversibility and cyclability of the Na plating/stripping reaction.

The morphologies and surface chemical compositions of the Na electrodes were investigated after 50 cycles. Parts (a) and (b) of Figure 6 present the surface SEM images of the Na electrodes cycled in a liquid electrolyte and GPE, respectively. The Na electrode with a liquid electrolyte exhibited a rough surface and nonuniformly deposited Na dendrite on the SEI layer. On the other hand, a relatively smooth surface without significant Na dendrite formation was observed for the Na electrode with GPE, indicating that GPE suppressed the Na dendrite growth and allowed uniform Na plating/stripping on the electrode surface. Figure 6c,d and Figure S6 show the XPS results of the Na electrodes after 50 cycles. We normalized all the XPS spectra with respect to the intensity of the Na Auger peak. The O 1s spectra showed five peaks, which can be assigned to $Na_2O$ (529.7 eV), $Na_2CO_3$ (531.6 eV), C−O group (532.8 eV), P−O group (533.3 eV), and C═O group (534.4 eV).[45,46] Five peaks corresponding to C−C, C−O, C═O, $ROCO_2Na$, and $Na_2CO_3$ species were observed at 285.0, 286.8, 288.0, 289.1, and 290.0 eV, respectively, in the C 1s spectra.[46] These chemical species result from the reductive decomposition of electrolyte components such as EC, PC, FEC, TMP, and NaFSI. The Na electrode cycled in GPE exhibited considerably lower peak intensities of C−O, P−O, C═O, and $Na_2CO_3$ species than the Na electrode with a


https://doi.org/10.1021/acsaem.1c02053
ACS Appl. Energy Mater. 2021, 4, 10153−10162

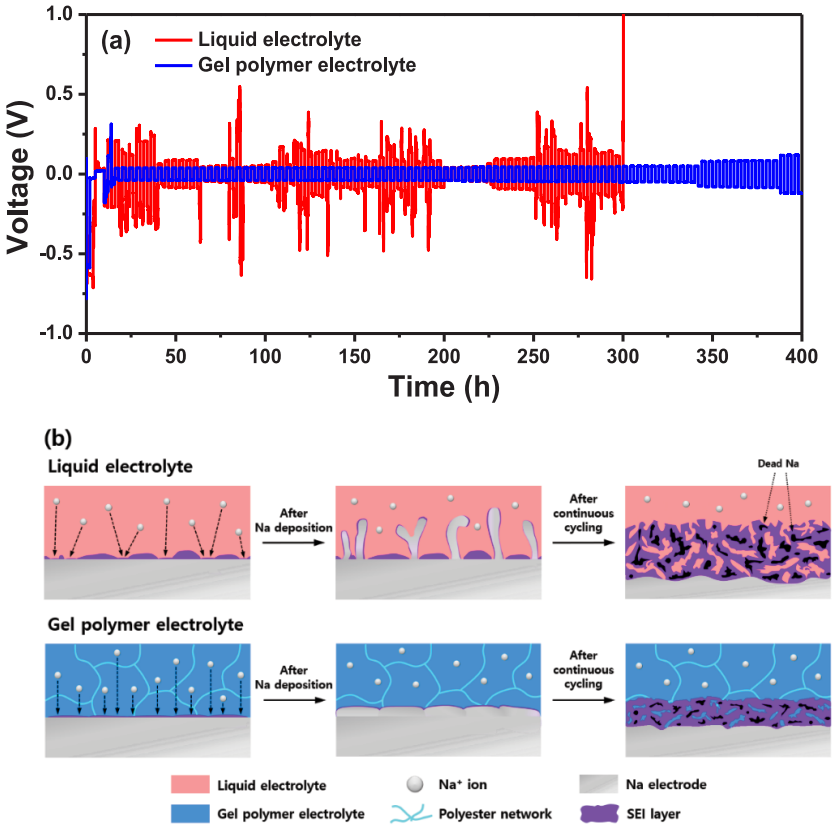


**Figure 5.** (a)Voltage profiles of the symmetrical Na/electrolyte/Na cells with different electrolytes at 0.5 mA $cm^{-2}$ for 2 h. (b) Schematic illustration of the dendritic Na growth and SEI formation on the Na electrode with liquid electrolyte (upper) and GPE (lower).

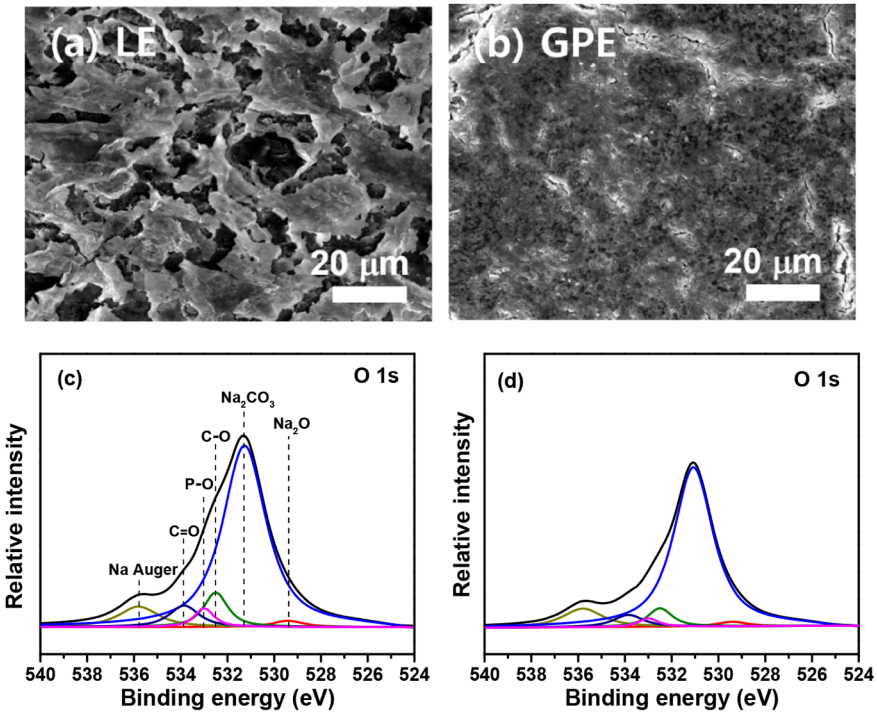


**Figure 6.** (a) SEM images of Na electrodes in (a) liquid electrolyte and (b) GPE after cycling at 0.5 mA $cm^{-2}$. O 1s XPS spectra of Na electrodes in (c) liquid electrolyte and (d) GPE after 50 cycles.

liquid electrolyte, confirming the suppressed electrolyte decomposition in the cell with GPE.

The $Na/Na_3V_2(PO_4)_3$ cell was assembled with an optimized GPE. The GPE precursor was injected into the cell and thermally cross-linked at 70 °C for 1 h. We investigated the



https://doi.org/10.1021/acsaem.1c02053
ACS Appl. Energy Mater. 2021, 4, 10153−10162

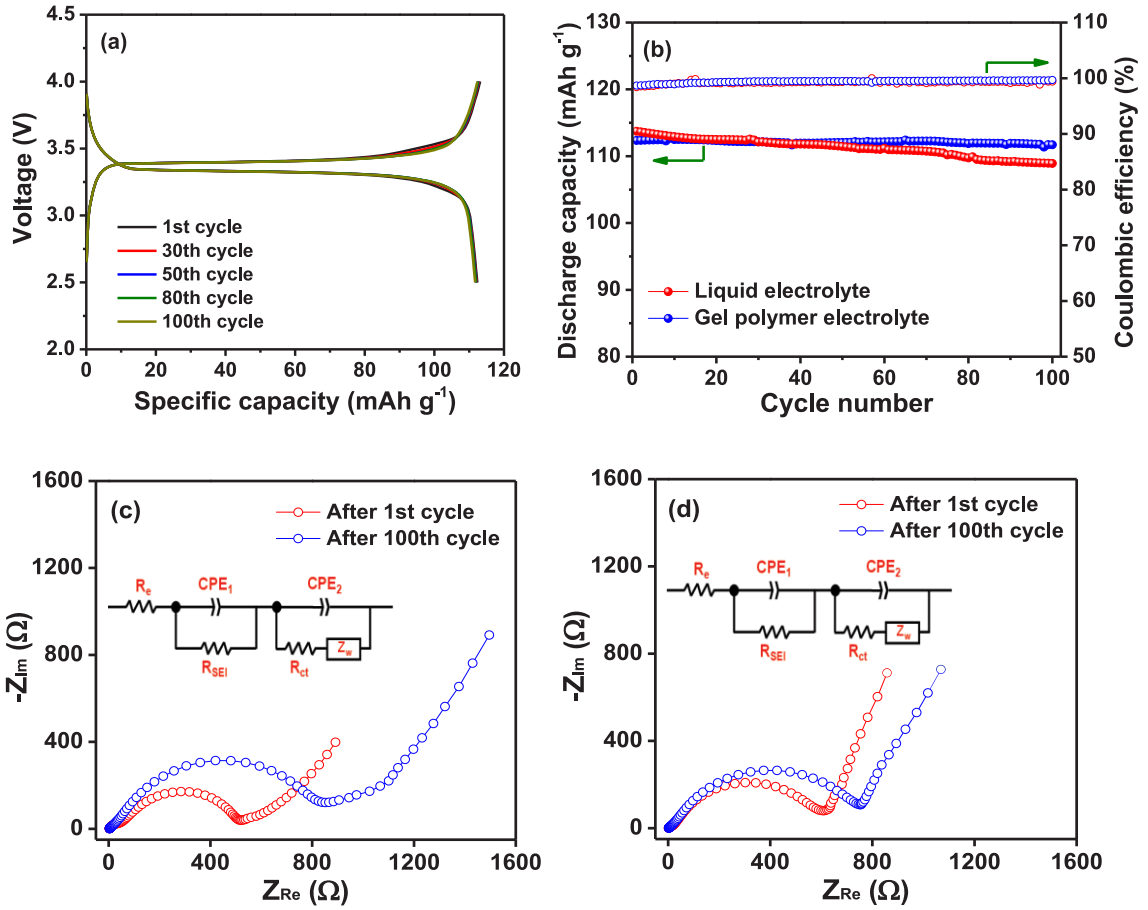


**Figure 7.** (a) Voltage profiles of the Na/$Na_3V_2(PO_4)_3$ cell with GPE at room temperature and a 0.25 C rate. (b) Cycling performance of the cells with different electrolytes at a 0.25 C rate. AC impedance spectra of the cells assembled with (c) liquid electrolyte and (d) GPE before and after cycling.

morphology of the PE-supported GPE, which was obtained by in situ cross-linking of gel precursor within the cell. Parts (a) and (b) of Figure S7 show the SEM images of the PE separator and PE-supported GPE, respectively. It can be clearly seen that the pores in the PE separator are fully covered and connected by GPE without any empty space. The electrochemical performance of Na/$Na_3V_2(PO_4)_3$ cells was investigated at a 0.25 C rate and at 25 °C. Figure 7a shows the voltage profiles of the cell assembled with GPE as a function of the cycle number. The cell exhibited a voltage plateau at approximately 3.4 V, which corresponds to the reversible transformation between $Na_3V_2(PO_4)_3$ and $NaV_2(PO_4)_3$.[30] The Na/$Na_3V_2(PO_4)_3$ cell showed stable cycling behavior without noticeable capacity fading. Figure 7b compares the cycling performance of the cells with different electrolytes. The cells with liquid electrolyte and GPE initially delivered discharge capacities of 113.7 and 112.3 mA h $g^{-1}$ based on the $Na_3V_2(PO_4)_3$ active material in the cathode, respectively. The discharge capacity of the liquid-electrolyte-based cell declined to 108.9 mA h $g^{-1}$ at 100 cycles. In contrast, the cell with GPE exhibited a high discharge capacity of 111.7 mA h $g^{-1}$ at 100 cycles, corresponding to a capacity retention of 99.4%. These results imply that the replacement of the liquid electrolyte with GPE can significantly improve the cycling stability of Na/$Na_3V_2(PO_4)_3$ cells. To gain further insight into the variation of internal resistance of the cells with cycling, we obtained AC impedance spectra of the Na/$Na_3V_2(PO_4)_3$ cells before and after cycling. The results are shown in Figure 7c,d along with a corresponding equivalent circuit. The liquid-electrolyte-based cell showed a large increase of interfacial resistance after the repeated cycling, which arises from the continuous electrolyte decomposition at the enlarged Na surface and the formation of a resistive passivation layer on the Na anode. In the Na/$Na_3V_2(PO_4)_3$ cell with GPE, the interfacial resistance slightly increased after cycling, indicating the stable interfacial characteristics between the Na electrode and GPE, as discussed above. Considering these results, the use of GPE is effective in maintaining a lower internal resistance in the cell and achieving stable cycling performance.

The rate performance of the Na/$Na_3V_2(PO_4)_3$ cells was evaluated at different C rates. Figure 8a and Figure S8a show the voltage profiles of the cells with GPE and a liquid electrolyte, respectively, which are obtained at current rates ranging from 0.1 to 3.0 C. The overpotential of the cell was gradually increased with the current rate. As a result, the discharge capacities of the Na/$Na_3V_2(PO_4)_3$ cells decreased with an increasing C rate from 0.1 to 3.0 C. Figure 8b compares the discharge capacities of the cells assembled with different electrolytes as a function of the C rate. The Na/$Na_3V_2(PO_4)_3$ cell with GPE exhibited comparable discharge capacities to the liquid-electrolyte-based cell at all current rates despite the lower ionic conductivity of GPE, which can be attributed to the favorable interfacial characteristics of GPE with electrodes. Figure 8c and Figure S8b show the discharge


https://doi.org/10.1021/acsaem.1c02053
ACS Appl. Energy Mater. 2021, 4, 10153−10162

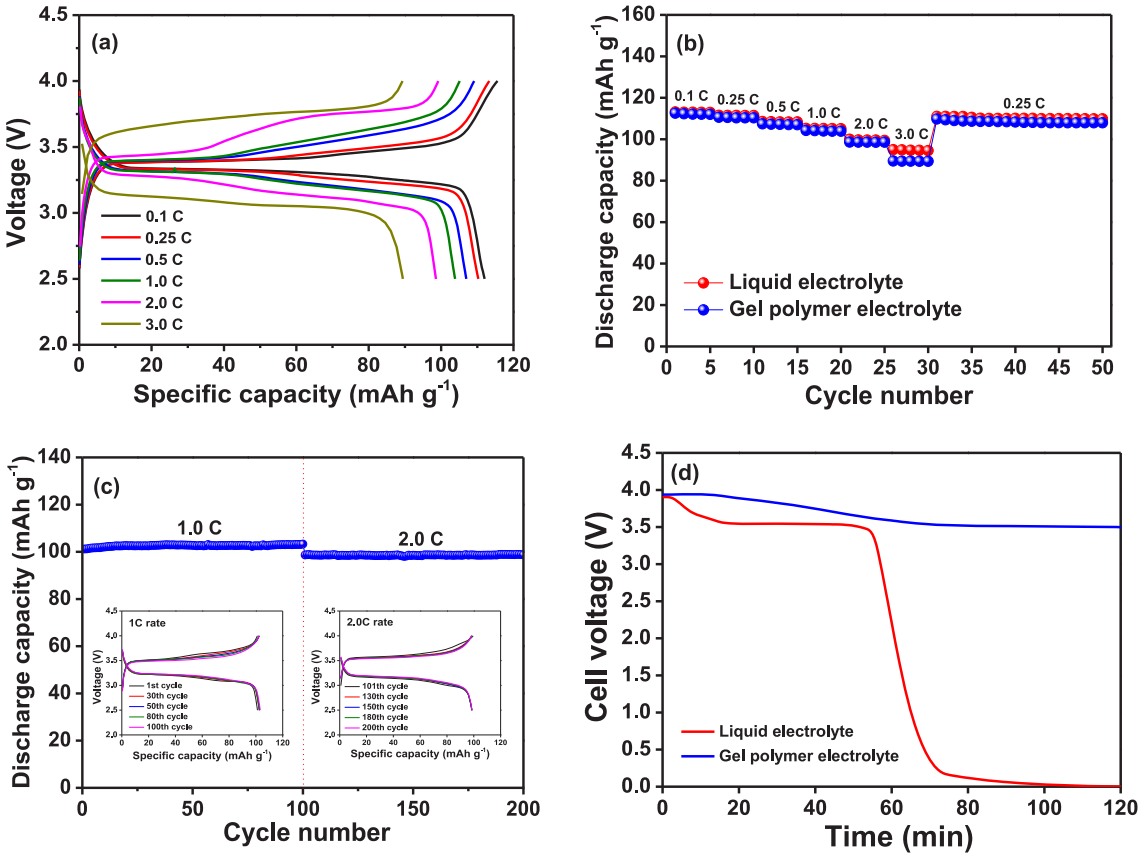


**Figure 8.** (a) Voltage profiles of the cell with GPE at different C rates. (b) Rate performance of the cells at various C rates. (c) Discharge capacities of the cell with GPE as a function of cycle number at 1.0 C and 2.0 C rates. (d) Variation of open-circuit voltages of the cells at 140 °C for 2 h.

capacities of the cells with GPE and the liquid electrolyte at high current rates. In the case of the liquid-electrolyte-based cell, the voltage fluctuation was observed during the charging process and the large capacity fading occurred, as depicted in Figure S8b. This result is related to the internal short circuit arising from the Na dendrite growth during the repeated cycling at high current rates. On the other hand, the cell with GPE delivered high discharge capacities and showed good capacity retention at 1.0 and 2.0 C rates. To investigate the long-term cycling stability of the GPE cell, it was further cycled at a 1.0 C rate after 200 cycles. As shown in Figure S9, the cell exhibited excellent cycling stability. These results indicate that the GPE synthesized by thermal cross-linking of ion-conductive PCL-TA is a reliable electrolyte system for achieving fast and stable cycling performance. The open-circuit voltage of the $Na/Na_3V_2(PO_4)_3$ cells was recorded during high-temperature storage at 140 °C. Before the test, the cells were fully charged to 4.0 V. As given in Figure 8d, the open-circuit voltage of the cell with the liquid electrolyte decreased to around 0 V after 1 h, which resulted from a short circuit of the cell due to large thermal shrinkage of the PE separator at 140 °C, as presented in Figure S10. On the other hand, the cell with GPE maintained a relatively stable cell voltage during high-temperature storage. Such superior thermal safety arises from the suppressed dimensional change of GPE (Figure S10) due to the formation of three-dimensional polymer networks in the GPE, which prevents a short circuit between the Na anode and $Na_3V_2(PO_4)_3$ cathode in the cell at high temperature. These results indicate that the superior thermal stability of the GPE synthesized by thermal cross-linking with PCL-TA allows safe operation of the cell at elevated temperatures.

## CONCLUSIONS

Nonflammable and cross-linked GPE was synthesized using ion-conductive PCL-TA to enhance the safety of sodium metal cells. In the GPE, the polyester network based on PCL effectively dissociated the Na salt because of the $Na^+$−carbonyl (ester) interactions and facilitated the ion conduction by a flexible polymer chain. GPE suppressed the electrolyte decomposition on the Na electrode by encapsulating a liquid electrolyte in the three-dimensional polymer network, which led to the formation of a thin SEI layer and uniform Na deposition on the Na electrode. With the combined effects of large amounts of free $Na^+$ ions and uniform Na deposition, the Na electrode cycled in the GPE exhibited a less dendritic structure during Na plating/stripping cycles. As a result, the sodium metal cell assembled with GPE exhibited excellent cycling stability and good rate capability. Our results demonstrate that the nonflammable GPE with a three-dimensional cross-linked structure can be a promising electrolyte system for safer and more stable operation of sodium metal cells.

## ASSOCIATED CONTENT

### Supporting Information

The Supporting Information is available free of charge at https://pubs.acs.org/doi/10.1021/acsaem.1c02053.

Schematic of the synthesis of PCL-TA; $^1H$ NMR spectra of PCL-triol and PCL-TA; photographs of GPEs during



https://doi.org/10.1021/acsaem.1c02053
ACS Appl. Energy Mater. 2021, 4, 10153−10162

flammability testing; ionic conductivities of GPEs and photographic images of GPEs during a flammability test; assignment of various Raman vibrational bands; time evolution of AC impedance spectra of the symmetrical Na/electrolyte/Na cells; C 1s XPS spectra of sodium electrodes disassembled from the symmetrical Na/electrolyte/Na cells; surface SEM images of a PE separator and PE-supported GPE; voltage profiles and discharge capacities of the cell with a liquid electrolyte at different C rates; discharge capacities of the cell with GPE as a function of cycle number at a 1.0 C rate; photographs of the PE separator and GPE before and after storage at 140 °C for 1 h (PDF)

## AUTHOR INFORMATION


### Corresponding Author

**Dong-Won Kim** − *Department of Chemical Engineering, Hanyang University, Seoul 04763, Republic of Korea;* orcid.org/0000-0002-1735-0272; Phone: +82 2 2220 2337; Email: dongwonkim@hanyang.ac.kr; Fax: +82 2 2298 4101

### Authors

**Tae-Hyun Park** − *Department of Chemical Engineering, Hanyang University, Seoul 04763, Republic of Korea*

**Myung-Soo Park** − *Department of Chemical Engineering, Hanyang University, Seoul 04763, Republic of Korea*

**A-Hyeon Ban** − *Department of Chemical Engineering, Hanyang University, Seoul 04763, Republic of Korea*

**Yun-Sung Lee** − *School of Chemical Engineering, Chonnam National University, Gwangju 61186, Republic of Korea;* orcid.org/0000-0002-6676-2871

Complete contact information is available at: https://pubs.acs.org/10.1021/acsaem.1c02053

### Author Contributions

#T.-H.P. and M.-S.P. contributed equally to this work.


### Notes

The authors declare no competing financial interest.

## ACKNOWLEDGMENTS

This work was supported by the National Research Foundation of Korea (NRF) funded by the Korean government (2019R1A4A2001527, 2021R1A2C2011050) and by the Technology Innovation Program (20012330) funded by the Ministry of Trade, Industry and Energy (MOTIE, Korea).

## REFERENCES


(1) Larcher, D.; Tarascon, J. M. Towards Greener and More Sustainable Batteries for Electrical Energy Storage. *Nat. Chem.* **2015**, *7*, 19−29.

(2) Kawamoto, H.; Tamaki, W. Trends in Supply of Lithium Resources and Demand of the Resources for Automobiles. *Sci. Technol. Trends, Quart. Rev.* **2011**, No. 39, 51.

(3) Yabuuchi, N.; Kubota, K.; Dahbi, M.; Komaba, S. Research Development on Sodium-Ion Batteries. *Chem. Rev.* **2014**, *114*, 11636−11682.

(4) Slater, M. D.; Kim, D.; Lee, E.; Johnson, C. S. Sodium-Ion Batteries. *Adv. Funct. Mater.* **2013**, *23*, 947−958.

(5) Hong, S. Y.; Kim, Y.; Park, Y.; Choi, A.; Choi, N.-S.; Lee, K. T. Charge Carriers in Rechargeable Batteries: Na Ions *vs.* Li Ions. *Energy Environ. Sci.* **2013**, *6*, 2067−2081.

(6) Hwang, J. Y.; Myung, S. T.; Sun, Y. K. Sodium-Ion Batteries: Present and Future. *Chem. Soc. Rev.* **2017**, *46*, 3529−3614.

(7) Dahbi, M.; Yabuuchi, N.; Fukunishi, M.; Kubota, K.; Chihara, K.; Tokiwa, K.; Yu, X.-f.; Ushiyama, H.; Yamashita, K.; Son, J.-Y.; Cui, Y.-T.; Oji, H.; Komaba, S. Black Phosphorus as a High-Capacity, High-Capability Negative Electrode for Sodium-Ion Batteries: Investigation of the Electrode/Electrolyte Interface. *Chem. Mater.* **2016**, *28*, 1625−1635.

(8) Komaba, S.; Murata, W.; Ishikawa, T.; Yabuuchi, N.; Ozeki, T.; Nakayama, T.; Ogata, A.; Gotoh, K.; Fujiwara, K. Electrochemical Na Insertion and Solid Electrolyte Interphase for Hard-Carbon Electrodes and Application to Na-Ion Batteries. *Adv. Funct. Mater.* **2011**, *21*, 3859−3867.

(9) De La Llave, E.; Borgel, V.; Park, K. J.; Hwang, J. Y.; Sun, Y. K.; Hartmann, P.; Chesneau, F. F.; Aurbach, D. Comparison Between Na-Ion and Li-Ion Cells: Understanding the Critical Role of the Cathodes Stability and the Anodes Pretreatment on the Cells Behaviors. *ACS Appl. Mater. Interfaces* **2016**, *8*, 1867−1875.

(10) Rui, X.; Sun, W.; Wu, C.; Yu, Y.; Yan, Q. An Advanced Sodium-Ion Battery Composed of Carbon Coated $Na_3V_2(PO_4)_3$ in a Porous Graphene Network. *Adv. Mater.* **2015**, *27*, 6670−6676.

(11) Che, H.; Chen, S.; Xie, Y.; Wang, H.; Amine, K.; Liao, X.-Z.; Ma, Z.-F. Electrolyte Design Strategies and Research Progress for Room-Temperature Sodium-Ion Batteries. *Energy Environ. Sci.* **2017**, *10*, 1075−1101.

(12) Zhou, D.; Liu, R.; Zhang, J.; Qi, X.; He, Y.-B.; Li, B.; Yang, Q.-H.; Hu, Y.-S.; Kang, F. In Situ Synthesis of Hierarchical Poly(ionic liquid)-Based Solid Electrolytes for High-Safety Lithium-Ion and Sodium-Ion Batteries. *Nano Energy* **2017**, *33*, 45−54.

(13) Xue, Z.; He, D.; Xie, X. Poly(ethylene oxide)-Based Electrolytes for Lithium-Ion Batteries. *J. Mater. Chem. A* **2015**, *3*, 19218−19253.

(14) Qi, X.; Ma, Q.; Liu, L.; Hu, Y.-S.; Li, H.; Zhou, Z.; Huang, X.; Chen, L. Sodium Bis(fluorosulfonyl)imide/Poly(ethylene oxide) Polymer Electrolytes for Sodium-Ion Batteries. *ChemElectroChem* **2016**, *3*, 1741−1745.

(15) Shin, W. K.; Cho, J.; Kannan, A. G.; Lee, Y.-S.; Kim, D.-W. Cross-Linked Composite Gel Polymer Electrolyte Using Mesoporous Methacrylate-Functionalized $SiO_2$ Nanoparticles for Lithium-Ion Polymer Batteries. *Sci. Rep.* **2016**, *6* (1), 26332.

(16) Lee, Y.-S.; Lee, J. H.; Choi, J.-A.; Yoon, W. Y.; Kim, D.-W. Cycling Characteristics of Lithium Powder Polymer Batteries Assembled with Composite Gel Polymer Electrolytes and Lithium Powder Anode. *Adv. Funct. Mater.* **2013**, *23*, 1019−1027.

(17) Gao, H.; Zhou, W.; Park, K.; Goodenough, J. B. A Sodium-Ion Battery with a Low-Cost Cross-Linked Gel-Polymer Electrolyte. *Adv. Energy Mater.* **2016**, *6*, 1600467.

(18) Park, M.-S.; Woo, H.-S.; Heo, J.-M.; Kim, J.-M.; Thangavel, R.; Lee, Y.-S.; Kim, D.-W. Thermoplastic Polyurethane Elastomer-Based Gel Polymer Electrolytes for Sodium-Metal Cells with Enhanced Cycling Performance. *ChemSusChem* **2019**, *12*, 4645−4654.

(19) Zheng, J.; Zhao, Y.; Feng, X.; Chen, W.; Zhao, Y. Novel safer phosphonate-based gel polymer electrolytes for sodium-ion batteries with excellent cycling performance. *J. Mater. Chem. A* **2018**, *6*, 6559−6564.

(20) Zheng, J.; Yang, Y.; Li, W.; Feng, X.; Chen, W.; Zhao, Y. Novel flame retardant rigid spirocyclic biphosphate based copolymer gel electrolytes for sodium ion batteries with excellent high-temperature performance. *J. Mater. Chem. A* **2020**, *8*, 22962−22968.

(21) Feng, J.; Lu, L. A Novel Bifunctional Additive for Safer Lithium-Ion Batteries. *J. Power Sources* **2013**, *243*, 29−32.

(22) Feng, J.; An, Y.; Ci, L.; Xiong, S. Nonflammable Electrolyte for Safer Non-Aqueous Sodium Batteries. *J. Mater. Chem. A* **2015**, *3*, 14539−14544.

(23) Xiao, L.; Zeng, Z.; Liu, X.; Fang, Y.; Jiang, X.; Shao, Y.; Zhuang, L.; Ai, X.; Yang, H.; Cao, Y.; Liu, J. Stable Li Metal Anode with "Ion-Solvent-Coordinated" Nonflammable Electrolyte for Safe Li Metal Batteries. *ACS Energy Lett.* **2019**, *4*, 483−488.

(24) Liu, X.; Jiang, X.; Zhong, F.; Feng, X.; Chen, W.; Ai, X.; Yang, H.; Cao, Y. High-Safety Symmetric Sodium-Ion Batteries Based on Nonflammable Phosphate Electrolyte and Double $Na_3V_2(PO_4)_3$ Electrodes. *ACS Appl. Mater. Interfaces* **2019**, *11*, 27833−27838.
(25) Wang, X.; Yasukawa, E.; Kasuya, S. Nonflammable Trimethyl Phosphate Solvent-Containing Electrolytes for Lithium-Ion Batteries: I. Fundamental Properties. *J. Electrochem. Soc.* **2001**, *148*, A1058−A1065.
(26) Jiang, X.; Liu, X.; Zeng, Z.; Xiao, L.; Ai, X.; Yang, H.; Cao, Y. A Nonflammable $Na^+$-Based Dual-Carbon Battery with Low-Cost, High Voltage, and Long Cycle Life. *Adv. Energy Mater.* **2018**, *8*, 1802176.
(27) Zeng, Z.; Murugesan, V.; Han, K. S.; Jiang, X.; Cao, Y.; Xiao, L.; Ai, X.; Yang, H.; Zhang, J.-G.; Sushko, M. L.; Liu, J. Non-Flammable Electrolytes with High Salt-to-Solvent Ratios for Li-Ion and Li-Metal Batteries. *Nat. Energy* **2018**, *3*, 674−681.
(28) Mogensen, R.; Colbin, S.; Menon, A. S.; Björklund, E.; Younesi, R. Sodium Bis(oxalate)borate in Trimethyl Phosphate: A Fire-Extinguishing, Fluorine-Free, and Low-Cost Electrolyte for Full-Cell Sodium-Ion Batteries. *ACS Appl. Energy Mater.* **2020**, *3*, 4974−4982.
(29) Park, S.; Jeong, B.; Lim, D.-A.; Lee, C. H.; Ahn, K. H.; Lee, J. H.; Kim, D.-W. Quasi-Solid-State Electrolyte Synthesized Using a Thiol−Ene Click Chemistry for Rechargeable Lithium Metal Batteries with Enhanced Safety. *ACS Appl. Mater. Interfaces* **2020**, *12*, 19553−19562.
(30) Thangavel, R.; Kaliyappan, K.; Kang, K.; Sun, X.; Lee, Y.-S. Going Beyond Lithium Hybrid Capacitors: Proposing a New High-Performing Sodium Hybrid Capacitor System for Next-Generation Hybrid Vehicles Made with Bio-Inspired Activated Carbon. *Adv. Energy Mater.,* **2016**, *6*, 1502199.
(31) Chen, S.; Feng, F.; Yin, Y.; Lizo, X.; Ma, Z. Plastic Crystal Polymer Electrolytes Containing Boron Based Anion Acceptors for Room Temperature All-Solid-State Sodium-Ion Batteries. *Energy Storage Materials* **2019**, *22*, 57−65.
(32) Bella, F.; Colo, F.; Nair, J. R.; Gerbaldi, C. Photopolymer Electrolytes for Sustainable, Upscalable, Safe, and Ambient-Temperature Sodium-Ion Secondary Batteries. *ChemSusChem* **2015**, *8*, 3668−3676.
(33) Park, M.-S.; Jung, Y.-C.; Kim, D.-W. Hybrid Solid Electrolytes Composed of Poly(1,4-butylene adipate) and Lithium Aluminum Germanium Phosphate for All-Solid-State $Li/LiNi_{0.6}Co_{0.2}Mn_{0.2}O_2$ cells. *Solid State Ionics* **2018**, *315*, 65−70.
(34) Liu, Q.; Wu, F.; Mu, D.; Wu, B. A theoretical study on $Na^+$ solvation in carbonate ester and ether solvents for sodium-ion batteries. *Phys. Chem. Chem. Phys.* **2020**, *22*, 2164−2175.
(35) Zhao, X. M.; Yan, Y.-W.; Ren, X.-X.; Chen, L.; Xu, S.-D.; Liu, S.-B.; Wang, X.-M.; Zhang, D. Trimethyl Phosphate for Nonflammable Carbonate-Based Electrolytes for Safer Room-Temperature Sodium-Sulfur Batteries. *ChemElectroChem* **2019**, *6*, 1229−1234.
(36) Quartarone, E.; Mustarelli, P. Electrolytes for Solid-State Lithium Rechargeable Batteries: Recent Advances and Perspectives. *Chem. Soc. Rev.* **2011**, *40*, 2525−2540.
(37) Seo, Y.; Jung, Y.-C.; Park, M.-S.; Kim, D.-W. Solid Polymer Electrolyte Supported by Porous Polymer Membrane for All-Solid-State Lithium Batteries. *J. Membr. Sci.* **2020**, *603*, 117995.
(38) Patra, J.; Huang, H.-T.; Xue, W.; Wang, C.; Helal, A. S.; Li, J.; Chang, J.-K. Moderately Concentrated Electrolyte Improves Solid−Electrolyte Interphase and Sodium Storage Performance of Hard Carbon. *Energy Storage Mater.* **2019**, *16*, 146−154.
(39) Shi, P.; Zheng, H.; Liang, X.; Sun, Y.; Cheng, S.; Chen, C.; Xiang, H. A highly Concentrated Phosphate-Based Electrolyte for High-Safety Rechargeable Lithium Batteries. *Chem. Commun.* **2018**, *54*, 4453−4456.
(40) Tchitchekova, D. S.; Monti, D.; Johansson, P.; Barde, F.; Randon-Vitanova, A.; Palacin, M. R.; Ponrouch, A. On the Reliability of Half-Cell Tests for Monovalent ($Li^+$, $Na^+$) and Divalent ($Mg^{2+}$, $Ca^{2+}$) Cation Based Batteries. *J. Electrochem. Soc.* **2017**, *164*, A1384.
(41) Yang, G.; Sacci, R. L.; Ivanov, I. N.; Ruther, R. E.; Hays, K. A.; Zhang, Y.; Cao, P.-F.; Veith, G. M.; Dudney, N. J.; Saito, T.; Hallinan, D. T.; Nanda, J. Probing Electrolyte Solvents at Solid/Liquid Interface Using Gap-Mode Surface-Enhanced Raman Spectroscopy. *J. Electrochem. Soc.* **2019**, *166*, A178.
(42) Woo, H.-S.; Moon, Y.-B.; Seo, S.; Lee, H.-T.; Kim, D.-W. Semi-Interpenetrating Polymer Network Composite Gel Electrolytes Employing Vinyl-Functionalized Silica for Lithium−Oxygen Batteries with Enhanced Cycling Stability. *ACS Appl. Mater. Interfaces* **2018**, *10*, 687−695.
(43) Zheng, X.; Bommier, C.; Luo, W.; Jiang, L.; Hao, Y.; Huang, Y. Sodium Metal Anodes for Room-Temperature Sodium-Ion Batteries: Applications, Challenges and Solutions. *Energy Storage Mater.* **2019**, *16*, 6−23.
(44) Lee, J.; Lim, H.-S.; Cao, X.; Ren, X.; Kwak, W.-J.; Rodríguez-Pérez, I. A.; Zhang, J.-G.; Lee, H.; Kim, H.-T. Lithium Dendrite Suppression with a Silica Nanoparticle-Dispersed Colloidal Electrolyte. *ACS Appl. Mater. Interfaces* **2020**, *12*, 37188−37196.
(45) Liu, X.; Jiang, X.; Zeng, Z.; Ai, X.; Yang, H.; Zhong, F.; Xia, Y.; Cao, Y. High Capacity and Cycle-Stable Hard Carbon Anode for Nonflammable Sodium-Ion Batteries. *ACS Appl. Mater. Interfaces* **2018**, *10*, 38141−38150.
(46) Kim, Y.-J.; Lee, H.; Noh, H.; Lee, J.; Kim, S.; Ryou, M.-H.; Lee, Y. M.; Kim, H.-T. Enhancing the Cycling Stability of Sodium Metal Electrodes by Building an Inorganic−Organic Composite Protective Layer. *ACS Appl. Mater. Interfaces* **2017**, *9*, 6000−6006.


https://doi.org/10.1021/acsaem.1c02053
*ACS Appl. Energy Mater.* 2021, 4, 10153−10162